

Interaction patterns and individual dynamics shape the way we move in synchrony

Francesco Alderisio[†], Gianfranco Fiore[†], Robin N. Salesse[‡],
Benoît G. Bardy^{‡§} & Mario di Bernardo^{†¶*}

The emergence of movement coordination in human ensembles has been seldom studied in the existing literature, in contrast to situations involving dual interaction. Here we investigate group synchronisation in a human ensemble where participants are asked to generate and coordinate an oscillatory hand motion. We separately test two groups of seven participants. We observe that the coordination level of the ensemble depends on the specific way each individual moves when isolated from the others, and on the pattern of the visual coupling among group members (who looks at whom). Despite the complexity of social interactions among individuals, we find that a network of heterogeneous Kuramoto oscillators captures and explains the group dynamics. Our findings can be relevant to any activity requiring the coordination of several people, as in music, sport or at work, and can be extended to account for other forms of interaction such as sound and feel.

[†]Department of Engineering Mathematics, Merchant Venturers Building, University of Bristol, Woodland Road, Clifton, Bristol BS8 1UB, United Kingdom (f.alderisio@bristol.ac.uk, gianfranco.fiore@bristol.ac.uk, m.dibernardo@bristol.ac.uk)

[‡]EuroMov, Montpellier University, 700 Avenue du Pic Saint-Loup, 34090 Montpellier, France (benoit.bardy@umontpellier.fr, salesse.robin@gmail.com)

[§]Institut Universitaire de France, 1 rue Descartes, 75231 Paris Cedex 05, France

[¶]Department of Electrical Engineering and Information Technology, University of Naples Federico II, Via Claudio 21, 80125 Naples, Italy (mario.dibernardo@unina.it)

Introduction

Many human activities involve coordination and cooperation between individuals performing a joint task. Natural examples include hands clapping in an audience [1], walking in a crowd [2, 3], music playing [4, 5] or sports [6, 7]. Achieving synchronisation in the group involves some form of interaction (sound, feel, vision), and the establishment of mental connectedness and social attachment among the group members. This phenomenon has been studied little in the existing literature, in contrast to the large number of results on the dynamics of animal groups [8, 9, 10, 11].

The available theoretical results on human coordination are mostly concerned with the case of two individuals performing a joint action [12, 13, 14, 15]; a recent example being that of the *mirror game* [16], presented as a paradigmatic case of study involving people imitating each other’s movements in a pair [17, 18]. For larger groups of individuals, some of the available experimental results include studies on rocking chairs [19, 20, 21], rhythmic activities and marching tasks [22], choir singers during a concert [23], group synchronisation of arm movements and respiratory rhythms [24], team rowing during a race [25] and other sport activities [26]. These studies analyse the emergence and the level of coordination in the group, but relate them neither to the structure of the interactions nor to the individual dynamics of the group members. Further studies show that the outcome and the quality of the performance in a number of situations strongly depend on how the individuals in the ensemble exchange visual, auditory and motor information [4, 27, 28, 29, 30, 31], but no systematic and quantitative study is presented of how specific interaction patterns affect coordination.

Here we confirm for the first time, experimentally and computationally, that different visual interaction patterns in the group affect the coordination level achieved by its members. We take as a paradigmatic example the case where participants are asked to generate an oscillatory hand motion and coordinate it with that of the others. We unfold the effects on synchronisation of heterogeneities in the individual motion characteristics of the participants (measured in terms of the intrinsic frequency of oscillation they generate in isolation). We convincingly show that **in order to maximise the level of coordination, people should be grouped according to the features characterising their motion in isolation, and that specific interconnections (i.e., topological structure) should be assigned**. For instance, we find that regardless of individual differences, some topologies (e.g., all-to-all) give rise to higher levels of synchronisation (defined as overall phase mismatch among agents), whereas for other topologies (e.g., consecutive dyads) better synchronisation is achieved through a higher homogeneity in individual dynamics. This confirms the empirical observations often made in human activities requiring team coordination. For example, it is known that in classical ballet an ideal location exists for each dancer to optimise visual exchanges within the group [32], or that in team rowing there may be an optimal way to choose the coxswain according to the natural internal tempi of the athletes, as s/he controls the rhythms of the rowers in order to achieve a better performance [33].

We complement our study with a data-driven mathematical model that captures the experimental observations. We show that, despite the complexity of unavoidable social interactions in the group [34, 35, 36, 37], when performing a simple oscillatory movement individuals behave as a network of heterogeneous Kuramoto oscillators [38, 39], where each equation is characterised by a different set of parameters to account for human-to-human variability. The model captures well the dependence of the coordination level in the group upon the intrinsic properties of its members and the interaction structure among them.

Results

In our experiments two groups of seven players were considered, respectively named Group 1 and Group 2. Members of each group were asked to perform a simple oscillatory movement with their preferred hand and to synchronise their motion (see *Methods*). The oscillations produced by each individual, when isolated from the others, had a specific natural frequency. The two groups of players exhibited a different level of dispersion with regards to their natural oscillation frequencies (measured in the absence of coupling, see Section 4 of Supplementary Information), as quantified by their respective coefficient of variations c_v (Figs 1a and 1b). In particular, the frequencies of Group 2 ($c_{v_2} = 21\%$) showed a higher dispersion than those of Group 1 ($c_{v_1} = 13\%$); (see also Supplementary Tables 1 and 2 in Supplementary Information.)

Four different topologies of interactions were implemented through visual coupling for each group: complete graph, ring graph, path graph and star graph (Fig. 2). For more details on the implementation of the interaction patterns, refer to Section 1 of Supplementary Information.

Group synchronisation depends on the interaction patterns and the natural oscillation frequencies of the players. The level of coordination in the group depends on the structure of the visual interaction patterns (Figs 1c and 1d). Also, it is influenced by the heterogeneity of the natural frequencies characterising the individual motion of the group members. Indeed, the *group synchronisation index* $\rho_g(t)$, equal to 1 in the ideal case of perfect coordination among all participants in the ensemble and taking lower values for increasing

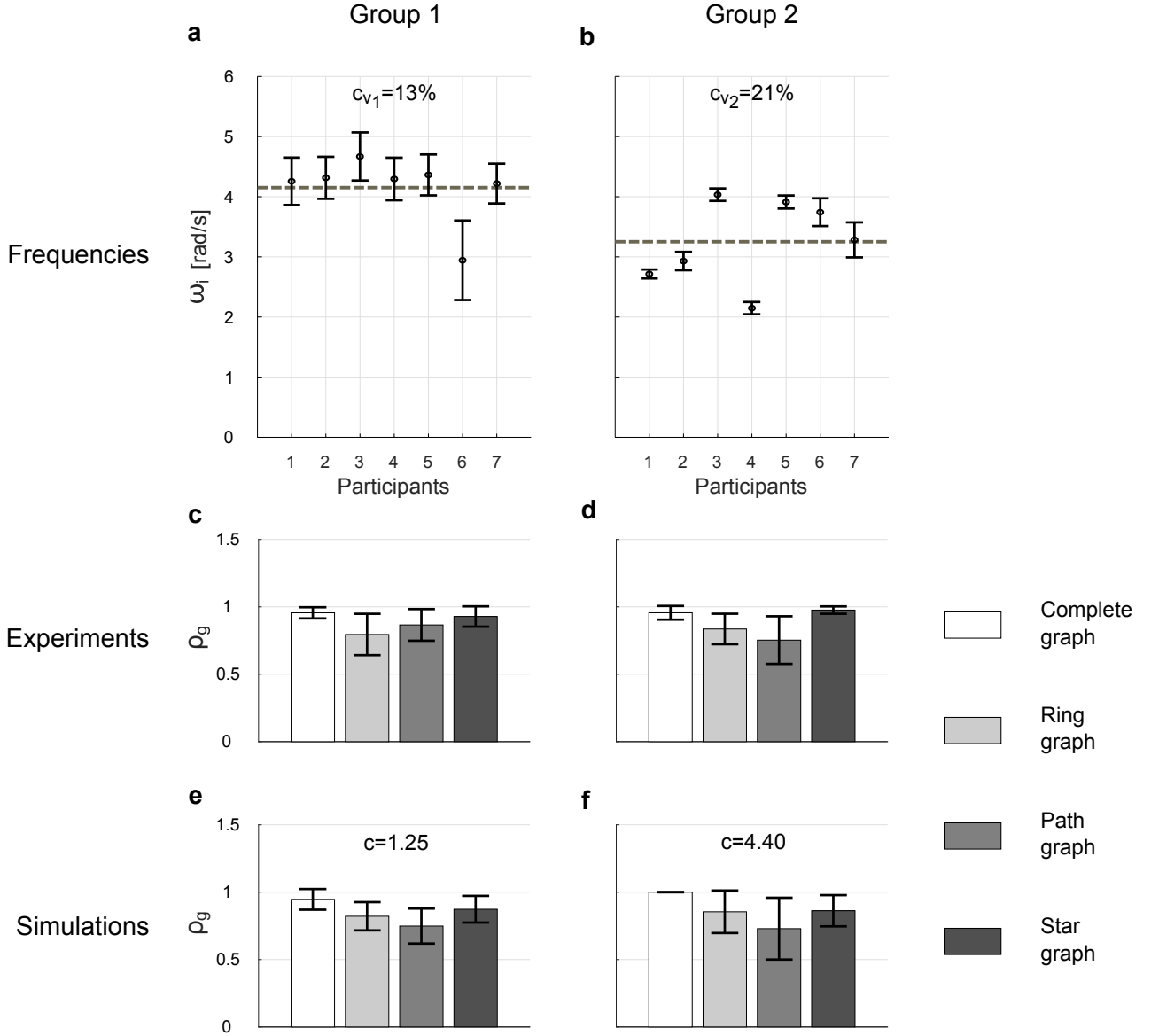


Figure 1: Natural oscillation frequencies and coordination level of the two groups. Mean (black circle) and standard deviation (black error bar) of the natural oscillation frequencies ω_i of the participants in Group 1 (a) and Group 2 (b) are presented. The frequencies of the latter are distributed further from their mean value averaged over the total number of players (grey dashed line) than those of the former, as quantified by their respective coefficient of variation c_v , which is equal to $c_{v_1} = 13\%$ for Group 1 and $c_{v_2} = 21\%$ for Group 2. As for the remaining panels, the height of each bar represents the mean value over time of the *group synchronisation index* averaged over the total number of trials, with different scales of grey referring to different topologies, whilst the black error bar represents its averaged standard deviation. Averaged mean value and standard deviation of $\rho_g(t)$ observed experimentally in Group 1 (c) and Group 2 (d) are presented, respectively. The *group synchronisation index* depends both on the interaction patterns and on the natural oscillation frequencies of the players: different values are obtained in the four implemented topologies within the same group, as well as for the same topology across the two different groups. These experimental observations are reproduced by simulating a network of heterogeneous Kuramoto oscillators. Averaged mean value and standard deviation of $\rho_g(t)$ obtained numerically for Group 1 (e) and Group 2 (f) are presented, respectively: the coupling strength in equation (1) is set to $c = 1.25$ to replicate the results of Group 1, and to $c = 4.40$ to replicate those of Group 2.

coordination mismatches (see Section 3 of Supplementary Information), is different in the four implemented topologies within the same group (with complete graph and star graph exhibiting the highest values), as well as for the same topology across the two different groups.

The experimental observations are well captured by the proposed mathematical model (Figs 1e and 1f). As

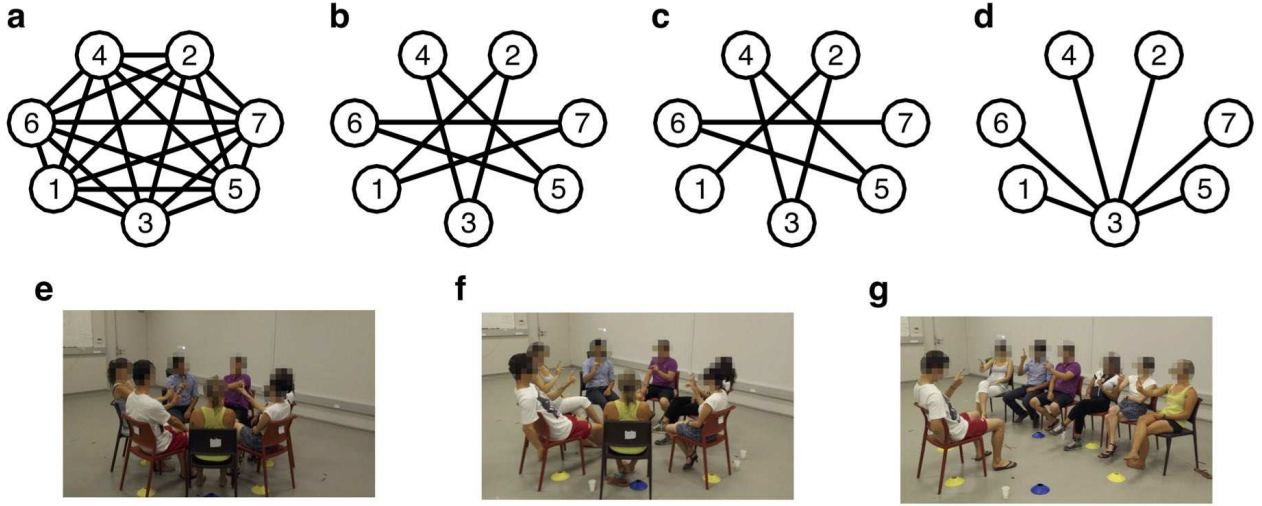


Figure 2: Interaction patterns implemented through visual coupling in the experiments. (a) Complete graph: each participant can see the movements of all the others. (b) Ring graph: each participant can see the movements of only her/his two *neighbours*. (c) Path graph: similar to the ring graph configuration, but agents 1 and 7, defined as *external*, have only one *neighbour* (2 and 6, respectively) and consequently are not visually coupled. (d) Star graph: agent 3, defined as *central*, can see the movements of all the others, defined as *peripheral*, who in turn see the movements of only the *central* player. The other panels show the actual arrangement of the players during the experiment [(e) for the complete graph, (f) for ring and path graphs, and (g) for the star graph].

expected, in order to reproduce the experiments (see also Section 5 of Supplementary Information for further details), the coupling strength c among the nodes in the model needs to take higher values for higher dispersions of the oscillation frequencies.

Visual coupling maximises synchronisation within connected dyads. For each participant of both groups, in most cases (99% for Group 1 and 94% for Group 2) the highest values of the *dyadic synchronisation indices* $\rho_{d_{h,k}}$, defined similarly to ρ_g but with respect to two generic participants h and k of the same group (see Section 3 of Supplementary Information), are observed for the visually connected dyads, a result that is found for all topologies (Fig. 3). For further details, refer to Section 6 of Supplementary Information.

The trend of $\rho_{d_{h,k}}$ is similar in both groups, with the only exception of the star graph in Group 1, where Player 7 did not manage to synchronise well with the *central* node (Fig. 3d, left panel). Note that in some cases, a relatively high value of ρ_g coexists with low values of $\rho_{d_{h,k}}$. For example, for Group 1 in the path graph configuration, we observe $\rho_g \simeq 0.87$ (Fig. 1c), while the dyadic synchronisation level between participants can be as low as $\rho_{d_{h,k}} \simeq 0.55$ (Fig. 3c, left panel). This suggests that overall group synchronisation can be high even though dyads who are not visually coupled do not exhibit equally high coordination levels.

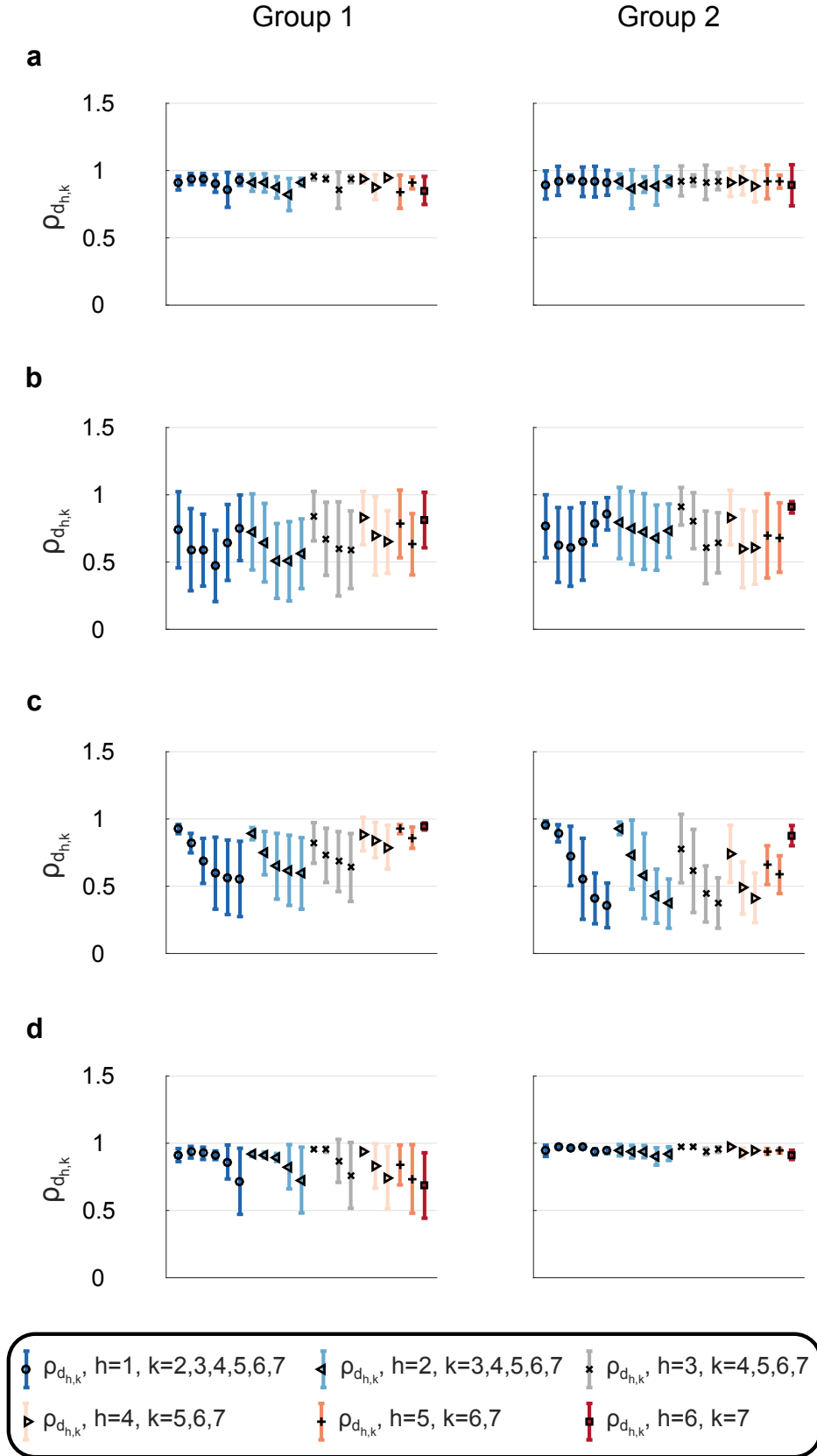


Figure 3: Dyadic synchronisations indices observed experimentally. Mean (symbol) and standard deviation (error bar) over the total number of trials of the *dyadic synchronisation index* $\rho_{d_{h,k}}$ for players of Group 1 (left panel) and Group 2 (right panel) in complete (a), ring (b), path (c) and star graph (d) are presented (the respective interaction patterns are shown in Fig. 2). Different symbols and colours refer to pairs related to different players: as the indices $\rho_{d_{h,k}}$ are symmetric by definition, only half of them are depicted. For each participant of both groups and in all the implemented topologies, the highest mean values are obtained for the visually connected dyads.

Discussion

In this work we studied synchronisation in multiplayer human ensembles. We asked two groups of seven volunteers to carry out a joint task in which they had to generate and synchronise an oscillatory motion of their preferred hand. We found that the coordination level among the players depended on *a)* their interaction patterns implemented through visual coupling and *b)* the natural oscillation frequencies of their individual motion. For *a)* we observed that the synchronisation levels in complete and star graphs were higher than those in path and ring graphs, thus revealing, for the first time in a human ensemble, the key theoretical finding in *Network Science* [40, 41] that synchronisation depends on the structure of the interconnections between agents in a network [42, 43, 44, 45, 46]. For *b)* we observed that the synchronisation level for a given topology was quantitatively different for the two groups characterised by a different dispersion of the agents' frequencies. In the particular case of the path graph, we found that the group whose members had natural frequencies closer to each other (Group 1) synchronised better. This extends to multiplayer scenarios the results of [47], which showed that greater interpersonal synchrony in musical duo performances is achieved when the endogenous rhythms of two pianists are closer to each other. Indeed, the path graph is the topology closest to dyadic interactions, as *external* agents have only one *neighbour* and the other agents have at most two *neighbours*.

More interestingly, despite the complexity of human social interactions, we found that a rather simple mathematical model of coupled Kuramoto oscillators was able to capture well the striking effects of the interaction structure and the intrinsic behaviour of the players on their synchronisation level. This can be instrumental for designing better architectures driving virtual agents, such as robots or computer avatars, to coordinate their motion within groups of humans [48, 49, 50, 51]. As expected from theory [52], we found that a higher value of coupling strength c in the model was necessary to reproduce the experimental observations in the case of more heterogeneous frequencies (higher c_v , Group 2). This can be interpreted as the need for greater attention by the human participants to synchronise their movements when their natural tempi are more heterogeneous. When, instead, their natural oscillation frequencies are closer (lower c_v , Group 1), participants synchronise with less effort, i.e., have to pay less attention in order to reach a good level of coordination.

Even though we studied a specific laboratory-oriented joint task, our approach reveals general principles behind the emergence of movement coordination in human groups that can apply to a large variety of contexts. As a specific example where our results find confirmation, it is worth mentioning the study on the coordination level (as measured by the same *group synchronisation index* we use here) of players in a football team, which is shown in [31] to depend on the defensive playing method (giving rise to different interaction patterns among the players) and on the players' dynamics when considering different teams.

Our study provides a criterion to determine the optimal players' arrangement in multi-agent scenarios (in terms of their individual behaviour), and to designate the optimal interconnections among them (structure of their interactions) in order to maximise coordination. This is a matter of crucial importance when a high level of coordination is required in a large ensemble. In music, the quality of the performance in an orchestra is related to the musicians playing in synchrony, and having all players pay attention to the conductor reproduces the star graph topology described above [37]. In collective sports, the overall performance can be improved when participants coordinate their movements [31]: in synchronised swimming, skating and dancing, the underlying structure of interactions resembles the complete graph topology, whereas in team rowing the disposition of the athletes resembles the path graph topology, with an external entrainment signal performed by the coxswain. Moreover, in recreational activities (e.g., our social Sunday jogging), health benefits and social affiliation might be greater when partners synchronise their pace [53]. Indeed, keeping the same natural rhythm maximises the time spent doing physical activity, thus allowing to reach an optimal trade-off between amount of calories burnt and enjoyable casual conversation.

As we further observed that high values of ρ_g can coexist with low values of $\rho_{d_{h,k}}$ for some pairs of agents, our results suggest that a good performance in certain group activities can also be achieved by making sure that high coordination levels are obtained only within specific pairs of participants appropriately coupled to each other.

Methods

Participants. A total of 14 volunteers participated in the experiments: 5 females and 9 males (5 participants were left handed). The majority of the participants were graduate and PhD students from the EuroMov research and innovation centre at the University of Montpellier in France. The experiments were held in two different sessions: seven participants took part in the first one and formed Group 1, the other seven participated in the second and formed Group 2.

The study was carried out according to the principles expressed in the Declaration of Helsinki and was approved by the local ethical committee (EuroMov, University of Montpellier). All participants provided written informed consent to participate in the study, and such consent was also approved by the ethical committee.

Task and procedure. Participants were asked to sit in a circle and move their preferred hand as smoothly as possible back and forth (i.e., away from and towards their bodies), along a direction required to be straight and parallel to the floor. Four different interaction patterns among players were implemented by asking each participant to focus their gaze on the motion of only a designated subset of other participants (for more details on the equipment employed and on how the different interaction structures were implemented see Section 1 of Supplementary Information).

- Complete graph (Figs 2a and 2e): participants were asked to keep their gaze focused on the middle of the circle in order to see the movements of all other participants.
- Ring graph (Figs 2b and 2f): each player was asked to maintain in her/his field of view the hand motion of only two other players, called *neighbours*.
- Path graph (Figs 2c and 2f): similar to the ring graph, but two participants, defined as *external* participants, were asked to maintain in their field of view the hand motion of only one *neighbour* (different for the two players).
- Star graph (Figs 2d and 2g): all participants but one sat side-by-side facing the remaining participant. The former, defined as *peripheral* players, were asked to focus their gaze on the motion of the latter, defined as *central* player, who in turn was asked to maintain in her/his field of view the hand motion of all others.

Each group performed the experiments in two different conditions:

1. *Eyes-closed condition.* Participants were asked to oscillate their preferred hand at their own comfortable tempo for 30-second trials (16 trials for Group 1 and 10 trials for Group 2) while keeping their eyes closed.
2. *Eyes-open condition.* Participants were asked to synchronise the motion of each other’s preferred hands during 30-second trials. For each topology, 10 trials lasting 30s each were performed.

Data acquisition and analysis. In order to detect the motion of the participants’ hands, circular markers were attached on top of their index finger. Eight infrared cameras (Nexus MX13 Vicon System ©) were located around the experimental room to record the position of the markers. For further details on how the experimental data was acquired and processed refer to Section 2 in Supplementary Information.

Synchronisation metrics. In order to quantify the synchronisation level in a network of more than two agents, the metrics introduced in [20] were used to characterise the quality and the level of coordination in the group. Such metrics were evaluated from the phases of the players’ movements, which in turn were estimated by making use of the Hilbert transform [54].

In particular, the coordination level of the two groups was measured at any time instant by means of the *group synchronisation index* $\rho_g(t) \in [0, 1]$, a time-varying quantity equal to 1 in the ideal case of perfect coordination at time t (no phase mismatch between all the agents in the network) and taking lower values for increasing phase mismatches, whereas the coordination level within any pair of participants in each group was assessed by means of the *dyadic synchronisation index* $\rho_{d_{h,k}} = \rho_{d_{k,h}}$, defined similarly to ρ_g but with respect to the synchronisation level between two generic participants h and k (refer to Section 3 of Supplementary Information for further details and mathematical definitions).

Networks of heterogeneous Kuramoto oscillators. The mathematical model proposed to account for the group synchronisation as observed experimentally is a network of heterogeneous Kuramoto oscillators [38]:

$$\dot{\theta}_i = \omega_i + \frac{c}{N} \sum_{j=1}^N a_{ij} \sin(\theta_j - \theta_i), \quad i = 1, 2, \dots, N \quad (1)$$

where θ_i is the phase of the motion of the preferred hand of the i -th human participant in the ensemble, ω_i is her/his own preferred oscillation frequency when not connected to any other partner (estimated from the eyes-closed trials), and N the number of participants. Each player is modelled with a different value of ω_i , thus accounting for human-to-human variability, and is affected by the interaction with her/his neighbours modelled by the second term in the right hand side of equation (1). Parameter c , here assumed to be constant and equal for all nodes in the network, models the interaction strength among the players, i.e., the strength of their mutual visual coupling. Finally, $a_{ij} = 1$ if there is a connection between players i and j (they are looking at each other in the eyes-open trials), while $a_{ij} = 0$ if there is not. Further information on how the model was initialised and parameterised can be found in Section 4 of Supplementary Information.

References

- [1] Néda, Z., Ravasz, E., Brechet, Y., Vicsek, T. & Barabási, A.-L. Self-organizing processes: The sound of many hands clapping. *Nature* **403(6772)**, 849-850 (2000).
- [2] Moussaïd, M., Perozo, N., Garnier, S., Helbing, D. & Theraulaz, G. The walking behaviour of pedestrian social groups and its impact on crowd dynamics. *PLoS ONE* **5(4)**, e10047 (2010).
- [3] Rio, K. & Warren, W. H. The visual coupling between neighbors in real and virtual crowds. *Transport. Res. Proc.* **2**, 132-140 (2014).
- [4] D'Ausilio, A. *et al.* Leadership in orchestra emerges from the causal relationships of movement kinematics. *PLoS ONE* **7(5)**, e35757 (2012).
- [5] Badino, L., D'Ausilio, A., Glowinski, D., Camurri, A. & Fadiga, L. Sensorimotor communication in professional quartets. *Neuropsychologia* **55**, 98-104 (2014).
- [6] Duch, J., Waitzman, J. S. & Amaral, L. A. N. Quantifying the performance of individual players in a team activity. *PLoS ONE* **5(6)**, e10937 (2010).
- [7] Silva, P. *et al.* Practice effects on intra-team synergies in football teams. *Hum. Movement Sci.* **46**, 39-51 (2016).
- [8] Couzin, I. D., Krause, J., Franks, N. R. & Levin, S. A. Effective leadership and decision-making in animal groups on the move. *Nature* **433(7025)**, 513-516 (2005).
- [9] Nagy, M., Ákos, Z., Biro, D. & Vicsek, T. Hierarchical group dynamics in pigeon flocks. *Nature* **464(7290)**, 890-893 (2010).
- [10] Nagy, M. *et al.* Context-dependent hierarchies in pigeons. *Proc. Natl. Acad. Sci. U.S.A.* **110(32)**, 13049-13054 (2013).
- [11] Zienkiewicz, A., Barton, D. A. W., Porfiri, M. & di Bernardo, M. Leadership emergence in a data-driven model of zebrafish shoals with speed modulation. *Eur. Phys. J. Spec. Top.* **224(17-18)**, 3343-3360 (2015).
- [12] Oullier, O., De Guzman, G. C., Jantzen, K. J., Lagarde, J. & Scott Kelso, J. A. Social coordination dynamics: Measuring human bonding. *Soc. Neurosci.* **3(2)**, 178-192 (2008).
- [13] Schmidt, R. C. & Turvey, M. T. Phase-entrainment dynamics of visually coupled rhythmic movements. *Biol. Cybern.* **70(4)**, 369-376 (1994).
- [14] Varlet, M., Marin, L., Lagarde, J. & Bardy, B. G. Social postural coordination. *J. Exp. Psychol. Hum. Percept. Perform.* **37(2)**, 473-483 (2011).
- [15] Słowiński, P. *et al.* Dynamic similarity promotes interpersonal coordination in joint action. *J. R. Soc. Interface* **13**, 20151093 (2016)
- [16] Noy, L., Dekel, E. & Alon, U. The mirror game as a paradigm for studying the dynamics of two people improvising motion together. *Proc. Natl. Acad. Sci. USA* **108(52)**, 20947-20952 (2011).
- [17] Zhai, C., Alderisio, F., Tsaneva-Atanasova, K. & di Bernardo, M. A novel cognitive architecture for a human-like virtual player in the mirror game. *Proc. IEEE Conf. Syst., Man, Cybern.* San Diego, California, USA. 754-759 (2014).
- [18] Zhai, C., Alderisio, F., Słowiński, P., Tsaneva-Atanasova, K. & di Bernardo, M. Design of a virtual player for joint improvisation with humans in the mirror game. *PLoS ONE* **11(4)**, e0154361 (2016).
- [19] Frank, T. D. & Richardson, M. J. On a test statistic for the Kuramoto order parameter of synchronization: an illustration for group synchronization during rocking chairs. *Phys. D* **239(23)**, 2084-2092 (2010).
- [20] Richardson, M. J., Garcia, R. L., Frank, T. D., Gergor, M. & Marsh, K. L. Measuring group synchrony: a cluster-phase method for analyzing multivariate movement time-series. *Front. Physiol.* **3** (2012).
- [21] Alderisio, F., Bardy, B. G. & di Bernardo, M. Entrainment and synchronization in networks of Rayleigh-van der Pol oscillators with diffusive and Haken-Kelso-Bunz couplings. *Biol. Cybern.* **110(2)**, 151-169, DOI: 10.1007/s00422-016-0685-7 (2016).
- [22] Iqbal, T. & Riek, L. A method for automatic detection of psychomotor entrainment. *IEEE T. Affect. Comput.* **7(1)**, 3-16 (2016)

- [23] Himberg, T. & Thompson, M. Group synchronization of coordinated movements in a cross-cultural choir workshop. *7th Triennial Conference of European Society for the Cognitive Sciences of Music* 175-180 (2009).
- [24] Codrons, E., Bernardi, N. F., Vandoni, M. & Bernardi, L. Spontaneous group synchronization of movements and respiratory rhythms. *PLoS ONE* **9(9)**, e107538 (2014).
- [25] Wing, A. M. & Woodburn, C. The coordination and consistency of rowers in a racing eight. *J. Sports Sci.* **13(3)**, 187-197 (1995).
- [26] Yokoyama, K. & Yamamoto, Y. Three people can synchronize as coupled oscillators during sports activities. *PLoS Comput. Biol.* **7(10)**, e1002181 (2011).
- [27] Healey, P. G. T., Leach, J. & Bryan-Kinns N. Inter-play: Understanding group music improvisation as a form of everyday interaction. *Proceedings of Less is More-Simple Computing in an Age of Complexity* (2005).
- [28] Kauffeld, S. & Meyers, R. A. Complaint and solution-oriented circles: Interaction patterns in work group discussions. *Eur. J. Work Organ. Psy.* **18(3)**, 267-294 (2009).
- [29] Passos, P. *et al.* Networks as a novel tool for studying team ball sports as complex social systems. *J. Sci. Med. Sport* **14(2)**, 170-176 (2011).
- [30] Duarte, R. *et al.* Intra-and inter-group coordination patterns reveal collective behaviors of football players near the scoring zone. *Hum. Mov. Sci.* **31(6)**, 1639-1651 (2012).
- [31] Duarte, R., Travassos, B., Araújo, D. & Richardson, M. J. *The influence of manipulating the defensive playing method on collective synchrony of football teams.* Performance Analysis of Sport IX. Routledge, Taylor & Francis Group London (2013).
- [32] Côté-Laurence, P. The role of rhythm in ballet training. *Res. Dance Educ.* **1(2)**, 173-191 (2000).
- [33] Schaffert, N., Mattes, K. & Effenberg, A. O. Listen to the boat motion: acoustic information for elite rowers. *Proc. Interactive Sonification Workshop* 31-38 (2010).
- [34] Baumeister, R. F. & Leary, M. R. The need to belong: desire for interpersonal attachments as a fundamental human motivation. *Psychol. Bull.* **117(3)**, 497-529 (1995).
- [35] Mäs, M., Flache, A. & Helbing, D. Individualization as driving force of clustering phenomena in humans. *PLoS Comput. Biol.* **6(10)**, e1000959 (2010).
- [36] Stark, T. H., Flache, A. & Veenstra, R. Generalization of positive and negative attitudes toward individuals to outgroup attitudes. *Pers. Soc. Psychol. B.* **39(5)**, 608-622 (2013).
- [37] Volpe, G., D'Ausilio, A., Badino, L., Camurri, A. & Fadiga, L. Measuring social interaction in music ensembles. *Phil. Trans. R. Soc. B.* **371**, 20150377 (2016).
- [38] Kuramoto, Y. *Chemical Oscillations, Waves and Turbulence.* Springer, Heidelberg (1984).
- [39] Strogatz, S. H. From Kuramoto to Crawford: exploring the onset of synchronization in populations of coupled oscillators. *Physica D* **143(1)** 1-20 (2000).
- [40] Albert, R. & Barabási, A.-L. Statistical mechanics of complex networks. *Rev. Mod. Phys.* **74(1)**, 47-97 (2002).
- [41] Newman, M., Barabási, A.-L & Watts, D. J. The structure and dynamics of networks. *Princeton University Press* (2011).
- [42] Arenas, A., Díaz-Guilera, A., Kurths, J., Moreno, Y. & Zhou, C. Synchronization in complex networks. *Phys. Rep.* **469(3)**, 93-153 (2008).
- [43] Assenza, S., Gutiérrez, R., Gómez-Gardeñes, J., Latora, V. & Boccaletti, S. Emergence of structural patterns out of synchronization in networks with competitive interactions. *Sci. Rep.* **1** (2011).
- [44] Moreno, Y. & Pacheco, A. F. Synchronization of Kuramoto oscillators in scale-free networks. *Europhys. Lett.* **68(4)**, 603 (2004).
- [45] Santos, F. C., Rodrigues, J. F. & Pacheco, J. M. Graph topology plays a determinant role in the evolution of cooperation. *Proc. R. Soc. Lond. [Biol]* **273(1582)**, 51-55 (2006).

- [46] Antonioni, A. & Cardillo, A. Coevolution of synchronization and cooperation in networks of coupled oscillators. arXiv preprint arXiv:1607.03186 (2016).
- [47] Zamm, A., Wellman, C. & Palmer, C. Endogenous rhythms influence interpersonal synchrony. *J. Exp. Psychol. Hum. Percept. Perform.* 1-6 (2016).
- [48] Zhai, C., Alderisio, F., Tsaneva-Atanasova, K. & di Bernardo, M. Adaptive tracking control of a virtual player in the mirror game. *Proc. IEEE Conf. Decis. Control* Los Angeles, California, USA. 7005-7010 (2014).
- [49] Zhai, C., Alderisio, F., Tsaneva-Atanasova, K. & di Bernardo, M. A model predictive approach to control the motion of a virtual player in the mirror game. *Proc. IEEE Conf. Decis. Control* Osaka, Japan. 3175-3180 (2015).
- [50] Boucenna, S., Cohen, D., Meltzoff, A. N., Gaussier, P. & Chetouani, M. Robots learn to recognize individuals from imitative encounters with people and avatars. *Sci. Rep.* **6** (2016).
- [51] Iqbal, T., Rack, S. & Riek, L. D. Movement coordination in human-robot teams: a dynamical systems approach. arXiv preprint arXiv:1605.01459 (2016).
- [52] DeLellis, P., di Bernardo, M. & Liuzza, D. Convergence and synchronization in heterogeneous networks of smooth and piecewise smooth systems. *Automatica* **56**, 1-11 (2015).
- [53] Marsh, K. L., Richardson, M. J. & Schmidt, R. C. Social connection through joint action and interpersonal coordination. *Top. Cogn. Sci.* **1(2)**, 320-339 (2009).
- [54] Kralemann, B., Cimponeriu, L., Rosenblum, M., Pikovsky, A. & Mrowka, R. Phase dynamics of coupled oscillators reconstructed from data. *Phys. Rev. E* **77(6)**, 066205 (2008).

Acknowledgements. The authors wish to acknowledge support from the European Project AlterEgo FP7 ICT 2.9 – Cognitive Sciences and Robotics, Grant Number 600610. The authors wish to thank Simon Pla (Montpellier University) for the help provided in running some of the experiments, Mathieu Gueugnon (Montpellier University) for providing some of the Matlab code necessary to analyse the data, and Prof. John Hogan (University of Bristol), Dr. Daniel Alberto Burbano Lombana (University of Naples Federico II) and Dr. Filippo Menolascina (the University of Edinburgh) for stimulating discussions and critical reading of the manuscript.

Author contributions. Conceived and designed the experiments: FA, RS, BB, MdB. Performed the experiments: FA, RS. Analysed the data: FA, GF. Contributed reagents/materials/analysis tools: FA, GF, RS. Wrote the paper: FA, GF, BB, MdB.

Competing financial interest. The authors declare no competing financial interest.

SUPPLEMENTARY INFORMATION

1 Experimental protocol

Participants were asked to sit in a circle on plastic chairs (Supplementary Fig. 4a) and move their preferred hand as smoothly as possible back and forth (that is, away from and back to their torso) on a plane parallel to the floor, along a direction required to be straight.

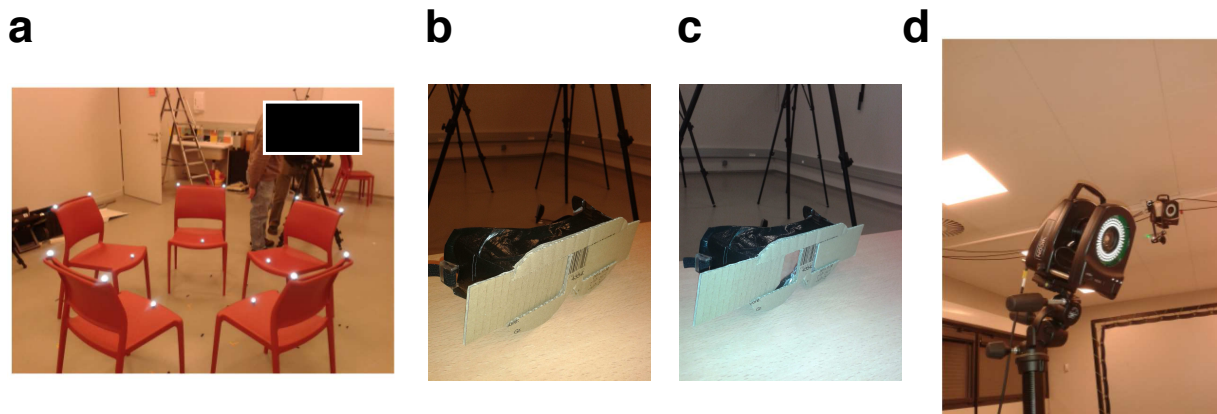


Figure 4: Experimental platform used for the experiments. (a) Plastic chairs with position markers. (b) Shut goggles: players are deprived of their own sight. (c) Open goggles: by appropriately sliding the mobile cardboard on the fixed one, players can modify their own field of view. (d) Eight cameras are employed to track the position of the hand of each player.

Different interaction patterns (also referred to in the text as interaction structure or topology) were implemented by asking each of the players to take into consideration the motion of only a designated subset of the other players. In order to physically implement these different interconnections, the field of view (FOV) of some players was reduced by means of *ad hoc* goggles. In particular, black duct tape was wrapped around such goggles in order to mask the peripheral FOV of the players on both sides. In addition, two cardboards, one of which was mobile, were appropriately glued on the goggles so as to restrict the FOV angle of each player by adjusting the position of the sliding cardboard (Supplementary Figs 4b and 4c). In such a way it was possible to implement different visual pairings among the players.

- **Complete graph** (Supplementary Figs 5a,e): participants sat in a circle facing each other without wearing the goggles. They were asked to keep their gaze focused on the middle of the circle in order to see the movements of all the others.
- **Ring graph** (Supplementary Figs 5b,f): participants sat in a circle facing each other while wearing the goggles. Each player was asked to see the hand motion of only two others, called *neighbours*. The goggles allowed participants to focus their gaze on the motion of their only two designated *neighbours*.
- **Path graph** (Supplementary Figs 5c,f): similar to the ring graph configuration, but two participants, defined as *external*, were asked to see the hand motion of only one *neighbour* (not the same). This was realised by removing the visual coupling between any pair of participants in the ring graph configuration.
- **Star graph** (Supplementary Figs 5d,g): all participants but one sat side by side facing the remaining participant while wearing the goggles. The former, defined as *peripheral* players, were asked to focus their gaze on the motion of the latter, defined as *central* player, who in turn was asked to see the hand motion of all the others.

2 Data analysis

In order to detect and analyse the three-dimensional position of the participants' hands, eight infrared cameras (Nexus MX13 Vicon System ©) were located around the experimental room (Supplementary Fig. 4d). Despite each of them achieving full frame synchronisation up to $350Hz$, data was recorded with a sampling frequency of $100Hz$, with an estimated error of $0.01mm$ for each coordinate.

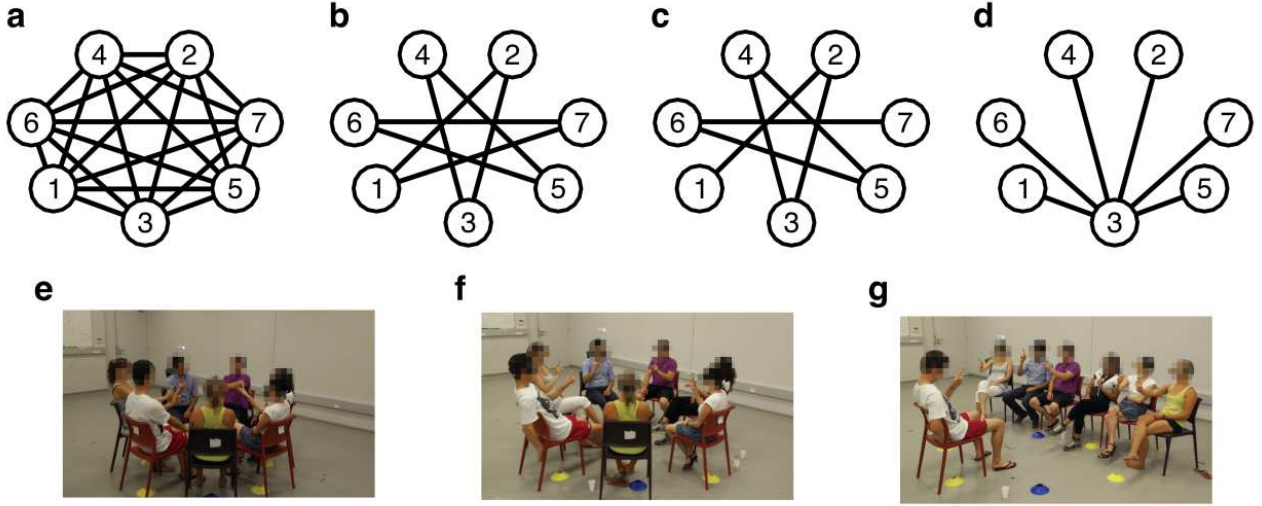


Figure 5: Interaction patterns implemented through visual coupling in the experiments. (a) Complete graph: each participant sees the movements of all the others. (b) Ring graph: each participant sees the movements of only her/his two *neighbours*. (c) Path graph: similar to the ring graph configuration, but agents 1 and 7, defined as *external*, have only one *neighbour* (2 and 6, respectively) and consequently are not visually coupled. (d) Star graph: agent 3, defined as *central*, sees the movements of all the others, defined as *peripheral*, who in turn see the movements of only the *central* player. The other panels show the actual arrangement of the players during the experiment [(e) for the complete graph, (f) for ring and path graphs, and (g) for the star graph]. Goggles are worn neither by all players in the complete graph, nor by the central player in the star graph.

In order for the cameras to detect the position of each player’s hand, circular markers were attached on top of their index fingers; such positions were provided as triplets of (x, y, z) coordinates in a Cartesian frame of reference (see Supplementary Fig. 6, black axes). In rare occasions (0.54% of the total number of data points for Group 1, never for Group 2) it was necessary to deprive these trajectories of possible undesired spikes caused by the cameras not being able to appropriately detect the position of the markers for the whole duration of the trial. As for Group 1, spikes were found in:

- 1 trajectory of Player 2 in the ring graph topology;
- 2 trajectories of Player 2 in the path graph topology;
- 4 trajectories of Player 2 and 8 trajectories of Player 7 in the star graph topology.

After removing possible spikes, classical interpolation techniques were used to fill the gap previously occupied by the spikes themselves. Besides, since the players’ positions were provided as triplets of (x, y, z) coordinates but essentially the motion of each player could be described as a one-dimensional movement, it was necessary to perform *principal component analysis* (PCA) on the collected trajectories to find such direction, which turns out to correspond to the x_{PCA} axis (see Supplementary Fig. 6, in red).

PCA was applied to the collected players’ trajectories defined by x and y , since the hand motion took place mostly in the (x, y) plane so that the z -coordinate could be neglected, obtaining the principal components x_{PCA} and y_{PCA} . Since the motion along the component y_{PCA} turns out to be negligible compared to that along x_{PCA} , it is possible to further assume that the motion of each player is one-dimensional (see Supplementary Fig. 7). For this reason, after removing possible spikes, all the data collected in the experiments underwent PCA and then only the first principal component, namely x_{PCA} , was considered for further analysis.

3 Synchronisation metrics

Let $x_k(t) \in \mathbb{R} \forall t \in [0, T]$ be the continuous time series representing the motion of each agent’s preferred hand, with $k \in [1, N]$, where N is the number of individuals and T is the duration of the experiment. Let $x_k[t_i] \in \mathbb{R}$, with $k \in [1, N]$ and $i \in [1, N_T]$, be the respective discrete time series of the k -th agent, obtained after sampling $x_k(t)$ at time instants t_i , where N_T is the number of time steps of duration $\Delta T := \frac{T}{N_T}$, that is the sampling period. Let $\theta_k(t) \in [-\pi, \pi]$ be the phase of the k -th agent, which can be estimated by making use of the Hilbert

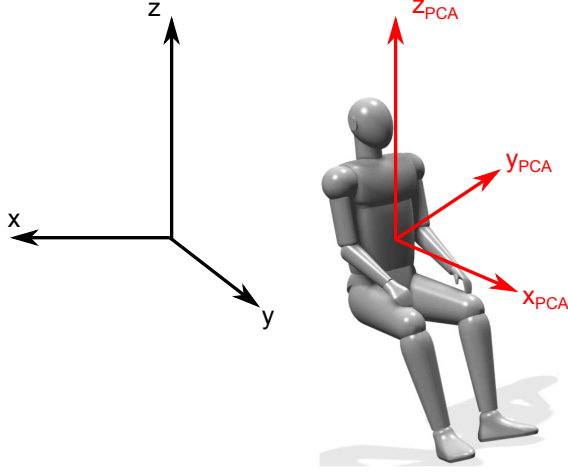


Figure 6: Cartesian frame of reference (x, y, z) and principal components $(x_{PCA}, y_{PCA}, z_{PCA})$. The axes x and y lie on a plane which is parallel to the ground, while the z axis is orthogonal to it. The axes x_{PCA} , y_{PCA} and z_{PCA} individuate the principal components: x_{PCA} is the direction where most of the movement takes place.

transform of the signal $x_k(t)$. We define the *cluster phase* or *Kuramoto order parameter*, both in its complex form $q'(t) \in \mathbb{C}$ and in its real form $q(t) \in [-\pi, \pi]$ as

$$q'(t) := \frac{1}{N} \sum_{k=1}^N e^{j\theta_k(t)}, \quad q(t) := \text{atan2}(\Im(q'(t)), \Re(q'(t))) \quad (2)$$

which can be regarded as the average phase of the group at time t .

Let $\phi_k(t) := \theta_k(t) - q(t)$ be the relative phase between the k -th participant and the group phase at time t . We can define the relative phase between the k -th participant and the group averaged over the time interval $[0, T]$, both in its complex form $\bar{\phi}'_k \in \mathbb{C}$ and in its real form $\bar{\phi}_k \in [-\pi, \pi]$ as

$$\bar{\phi}'_k := \frac{1}{T} \int_0^T e^{j\phi_k(t)} dt \simeq \frac{1}{N_T} \sum_{i=1}^{N_T} e^{j\phi_k[t_i]}, \quad \bar{\phi}_k := \text{atan2}(\Im(\bar{\phi}'_k), \Re(\bar{\phi}'_k)) \quad (3)$$

In order to quantify the synchronisation level of the entire group at time t we define the following parameter

$$\rho_g(t) := \frac{1}{N} \left| \sum_{k=1}^N e^{j(\phi_k(t) - \bar{\phi}_k)} \right| \in [0, 1] \quad (4)$$

as the *group synchronisation index*: the closer $\rho_g(t)$ is to 1, the smaller the average phase mismatch of the agents in the group at time t . Its value can be averaged over the whole time interval $[0, T]$ in order to have an estimate of the mean synchronisation level of the group during the total duration of the performance:

$$\rho_g := \frac{1}{T} \int_0^T \rho_g(t) dt \simeq \frac{1}{N_T} \sum_{i=1}^{N_T} \rho_g[t_i] \in [0, 1] \quad (5)$$

Moreover, if we denote with $\phi_{d_{h,k}}(t) := \theta_h(t) - \theta_k(t)$ the relative phase between two participants in the group at time t , it is possible to define the following parameter

$$\rho_{d_{h,k}} := \left| \frac{1}{T} \int_0^T e^{j\phi_{d_{h,k}}(t)} dt \right| \simeq \left| \frac{1}{N_T} \sum_{i=1}^{N_T} e^{j\phi_{d_{h,k}}(t_i)} \right| \in [0, 1] \quad (6)$$

as their *dyadic synchronisation index*: the closer $\rho_{d_{h,k}}$ is to 1, the lower the phase mismatch between agents h and k over the whole trial.

4 Parameterisation and initialisation of the mathematical model

In order to capture the experimental observations, we use the mathematical model

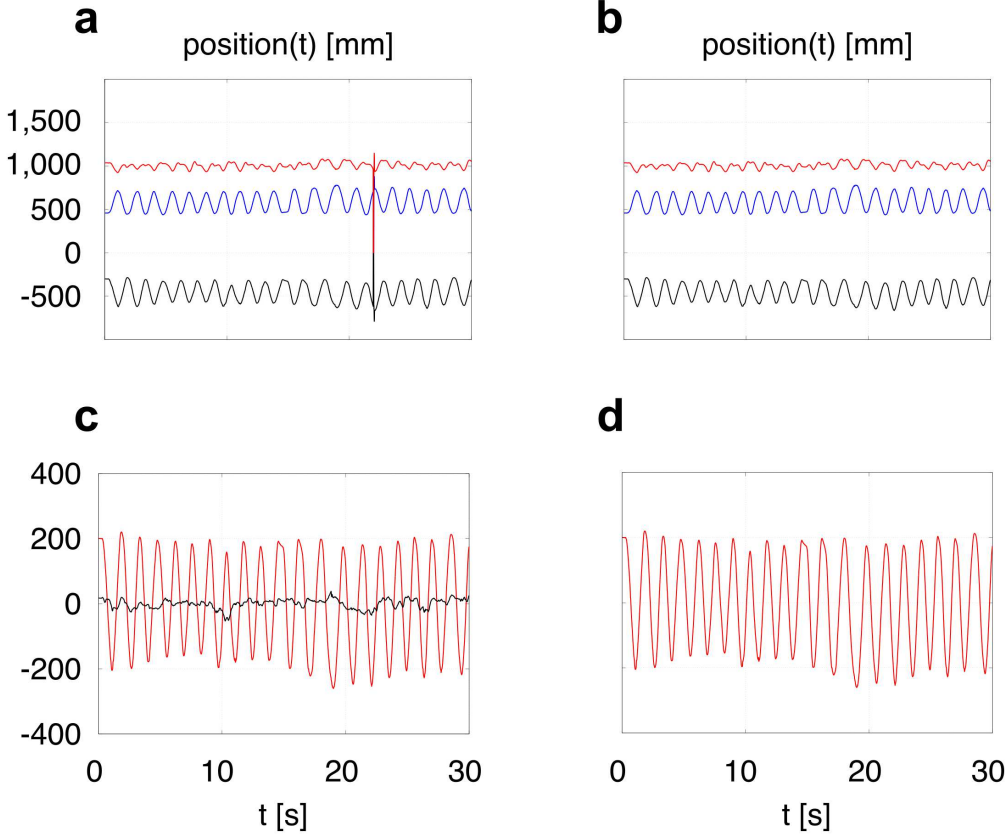


Figure 7: Pre-analysis for the hand motion of a given participant. (a) Original trajectories defined by (x, y, z) , respectively represented in blue, black and red, after recording the hand motion of each participant. (b) Trajectories (x, y, z) , respectively represented in blue, black and red, after removing the spikes. (c) Trajectories (x_{PCA}, y_{PCA}) , respectively represented in red and black, after PCA analysis applied onto x and y . (d) One-dimensional trajectory, defined by x_{PCA} (in red), used for further analysis.

$$\dot{\theta}_i = \omega_i + \frac{c}{N} \sum_{j=1}^N a_{ij} \sin(\theta_j - \theta_i), \quad i = 1, 2, \dots, N \quad (7)$$

where θ_i is the phase of the motion of the preferred hand of the i -th human participant in the ensemble, ω_i is her/his own natural oscillation frequency when not connected to any other partner (estimated from the eyes-closed trials), and N the number of participants. Each player is modelled with a different value of ω_i , thus accounting for human-to-human variability, and is affected by the interaction with her/his neighbours modelled by the second term in the right-hand side of Supplementary equation (7). The parameter c , here assumed to be constant and equal for all the nodes in the network, models the interaction strength among the players, i.e. the strength of their mutual visual coupling. Finally, $a_{ij} = 1$ if there is a connection between players i and j (they are looking at each other in the eyes-open trials), while $a_{ij} = 0$ if there is not.

The values of the natural oscillation frequencies ω_i were estimated by considering the M eyes-closed trials performed by the human players ($M = 16$ for Group 1, and $M = 10$ for Group 2). In particular, we evaluated the highest harmonic of each player's motion, thus obtaining M values for each participant. For our simulations, we assumed that each angular velocity ω_i of Supplementary equation (7) was a time-varying quantity, randomly extracted from a normal distribution whose mean and standard deviation are evaluated from the M aforementioned values collected for each human participant (see Supplementary Table 1 for more details on Group 1, and Supplementary Table 2 for Group 2).

If we define $\tilde{\omega} := [\mu(\omega_1) \ \mu(\omega_2) \ \dots \ \mu(\omega_7)]^T \in \mathbb{R}^7$, such values of frequencies lead to a coefficient of variation $c_v := \frac{\sigma(\tilde{\omega})}{\mu(\tilde{\omega})}$ equal to $c_{v_1} \simeq 0.13$ for Group 1, and $c_{v_2} \simeq 0.21$ for Group 2.

As for the coupling strength c , we found that setting the same constant value for all the topologies under investigation captures well the experimental observations (see Supplementary Section 5 below). As for the initial values of the phases, since before starting any trial all the human players were asked to completely extend their arm so that the first movement would be pulling their arm back towards their torso from the same initial conditions, we set $\theta_i(0) = \frac{\pi}{2}$ for all the nodes, trials and topologies.

Table 1: Mean value and standard deviation, over the total number of eyes-closed trials, of the players’ natural oscillation frequencies – Group 1.

Player	$\mu(\omega_i)$	$\sigma(\omega_i)$
1	4.2568	0.3941
2	4.3143	0.3492
3	4.6691	0.3999
4	4.2951	0.3543
5	4.3623	0.3406
6	2.9433	0.6609
7	4.2184	0.3314

The mean value of the frequencies is indicated with $\mu(\omega_i)$, while their standard deviation is indicated with $\sigma(\omega_i)$, $\forall i \in [1, N]$.

Table 2: Mean value and standard deviation, over the total number of eyes-closed trials, of the players’ natural oscillation frequencies – Group 2.

Player	$\mu(\omega_i)$	$\sigma(\omega_i)$
1	2.7151	0.0741
2	2.9299	0.1525
3	4.0344	0.1035
4	2.1476	0.1023
5	3.9117	0.1085
6	3.7429	0.2309
7	3.2827	0.2911

The mean value of the frequencies is indicated with $\mu(\omega_i)$, while their standard deviation is indicated with $\sigma(\omega_i)$, $\forall i \in [1, N]$.

5 Group synchronisation

For each of the two groups we show the *group synchronisation index* obtained experimentally and numerically by simulating the model proposed in Supplementary equation (7), with two different values of coupling strength c heuristically found by trial-and-error (Supplementary Fig. 8 and Supplementary Table 3 for Group 1, and Supplementary Fig. 9 and Supplementary Table 4 for Group 2). It is possible to appreciate how a low (or high) value of c in the model reproduces well the experimental observations in the case of lower (or higher) heterogeneity in the natural oscillation frequencies of the agents. On the other hand, experiments are not well reproduced when:

- the natural oscillation frequencies of the agents are close to each other and the coupling strength is too high ($c = 4.40$ for Group 1, the coordination level in the star graph should be higher than that in the ring graph);
- the natural oscillation frequencies of the agents are far from each other and the coupling strength is too low ($c = 1.25$ for Group 2, the coordination level in ring, path and star graph is not comparable with that obtained experimentally).

Table 3: Mean value $\mu(\rho_g)$ and standard deviation $\sigma(\rho_g)$ over time of the *group synchronisation index*, averaged over the total number of eyes-open trials – Group 1.

Topology	Experiments	Simulations, $c = 1.25$	Simulations, $c = 4.40$
Complete graph	0.9556 ± 0.0414	0.9468 ± 0.0767	0.9999 ± 0.0003
Ring graph	0.7952 ± 0.1532	0.8214 ± 0.1047	0.9575 ± 0.0740
Path graph	0.8661 ± 0.1173	0.7486 ± 0.1300	0.8288 ± 0.1636
Star graph	0.9285 ± 0.0753	0.8735 ± 0.0990	0.9052 ± 0.0940

This table shows $\mu(\rho_g) \pm \sigma(\rho_g)$ for both experimental and simulation results.

Group 1, $c_{v_1}=13\%$

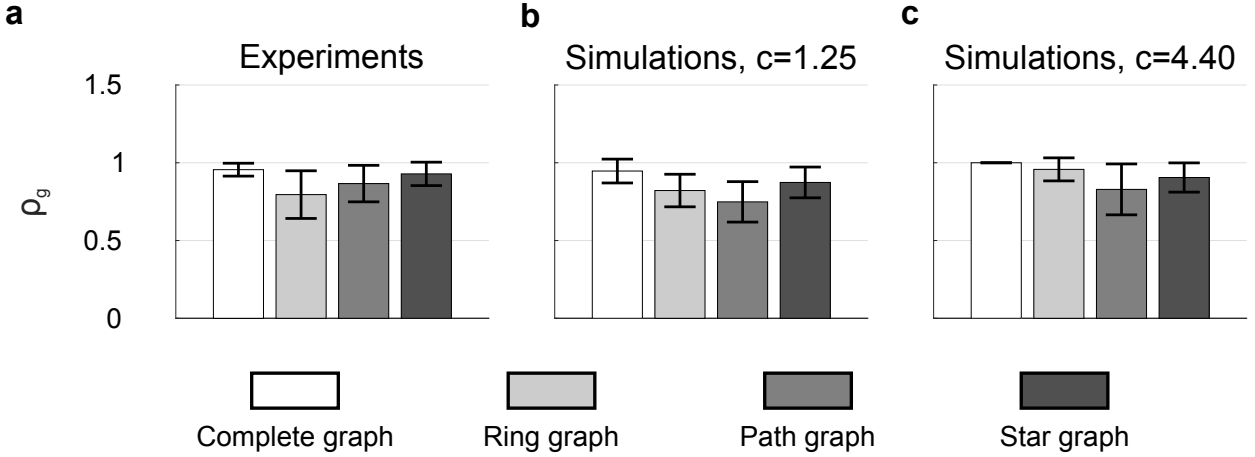


Figure 8: Coordination level of Group 1. The height of each bar represents the mean value over time of $\rho_g(t)$ averaged over the total number of eyes-open trials, with different scales of grey referring to different topologies, whilst the black error bar represents its averaged standard deviation. The group synchronisation indices obtained experimentally across the four implemented topologies (a) are captured well numerically when $c = 1.25$ (b), while they are not when $c = 4.40$ (c).

Table 4: Mean value $\mu(\rho_g)$ and standard deviation $\sigma(\rho_g)$ over time of the *group synchronisation index*, averaged over the total number of eyes-open trials – Group 2.

Topology	Experiments	Simulations, $c = 4.40$	Simulations, $c = 1.25$
Complete graph	0.9559 ± 0.0508	0.9999 ± 0.0004	0.9338 ± 0.0863
Ring graph	0.8358 ± 0.1130	0.8546 ± 0.1577	0.4764 ± 0.2157
Path graph	0.7534 ± 0.1766	0.7295 ± 0.2292	0.4771 ± 0.2064
Star graph	0.9759 ± 0.0274	0.8623 ± 0.1158	0.5447 ± 0.1740

This table shows $\mu(\rho_g) \pm \sigma(\rho_g)$ for both experimental and simulation results.

6 Dyadic synchronisations

For both Group 1 and Group 2, we show mean values and standard deviations of $\rho_{d_{h,k}}$ over the 10 eyes-open trials of each topology. In particular, if we denote with $\rho_{d_{h,k}}^{(l)}$ the value of the *dyadic synchronisation index* $\rho_{d_{h,k}}$ in the l -th trial of a certain topology, the mean value over the total number of trials is given by

$$\rho_{\mu,hk} = \frac{1}{10} \sum_{l=1}^{10} \rho_{d_{h,k}}^{(l)} \quad (8)$$

Similarly, the standard deviation is given by

$$\rho_{\sigma,hk} = \sqrt{\frac{1}{10} \sum_{l=1}^{10} \left(\rho_{d_{h,k}}^{(l)} - \rho_{\mu,hk} \right)^2} \quad (9)$$

For both Group 1 and Group 2, mean values and standard deviations of the *dyadic synchronisation index* are shown for all the pairs in the four implemented topologies (Supplementary Fig. 10). For the sake of clarity, all values of $\rho_{\mu,hk}$ and $\rho_{\sigma,hk}$ are expressed as percentiles (multiplied by 100). In most cases (99% for Group 1 and 94% for Group 2) the highest mean values of the dyadic synchronisation indices are observed for the visually connected dyads (represented in bold in Supplementary Fig. 10), meaning that players managed to maximise synchronisation with their visually coupled partners.

In particular:

- Complete graph: all means $\rho_{\mu,hk}$ are higher than 0.82 for Group 1 and 0.86 for Group 2.

Group 2, $c_{v_2}=21\%$

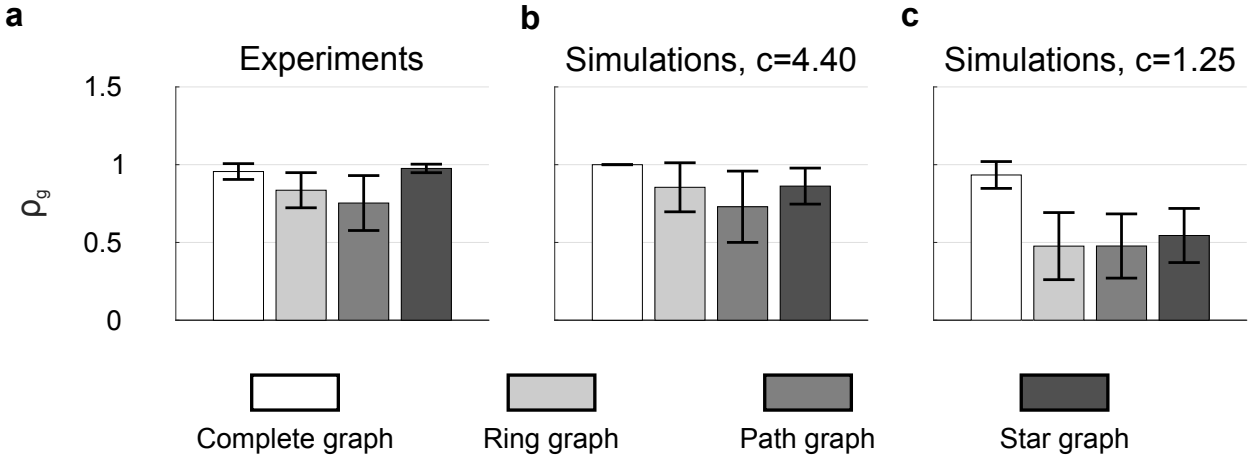


Figure 9: Coordination level of Group 2. The height of each bar represents the mean value over time of $\rho_g(t)$ averaged over the total number of eyes-open trials, with different scales of grey referring to different topologies, whilst the black error bar represents its averaged standard deviation. The group synchronisation indices obtained experimentally across the four implemented topologies (a) are captured well numerically when $c = 4.40$ (b), while they are not when $c = 1.25$ (c).

- Ring graph: for each player of Group 1 the highest values of $\rho_{\mu,hk}$ are obtained with respect to the two agents that player was asked to be topologically connected with, whereas for each player of Group 2 at least either of the two values of $\rho_{\mu,hk}$ related to her/his *neighbours* turns out to be the highest, and that related to the other *neighbour* is either the second highest (nodes 2, 4 and 7), the third highest (nodes 1, 3 and 6) or the fourth highest (node 5).
- Path graph: remarks analogous to those of the ring graph configuration can be made. The only exception is node 4 for Group 1, where $\rho_{\mu,43} < \rho_{\mu,46}$ (however the two values are still close to each other, as $\rho_{\mu,43} = \rho_{\mu,34} = 0.82$ and $\rho_{\mu,46} = \rho_{\mu,64} = 0.84$), and node 3 for Group 2, where $\rho_{\mu,34} = \rho_{\mu,43} = 0.78$ is lower than $\rho_{\mu,31} = \rho_{\mu,13} = 0.89$. It is also worth pointing out how, for both groups, consistently with the implemented network of interactions, the mean values $\rho_{\mu,17} = \rho_{\mu,71}$ are lower than those corresponding to the ring graph configuration, which is a consequence of removing the visual coupling between the *external* agents 1 and 7.
- Star graph: for each *peripheral* player of both the groups, the highest values of $\rho_{\mu,hk}$ are obtained with respect to Player 3 (*central* player).

As for the standard deviations $\rho_{\sigma,hk}$, in most cases (86% for Group 1 and 89% for Group 2) the lowest values are observed for the topologically connected dyads (represented in bold in Supplementary Fig. 10), which confirms the robustness of the interactions between visually coupled pairs.

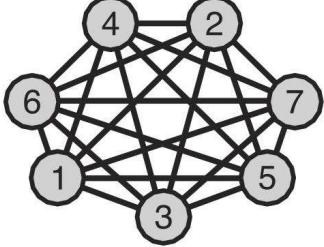
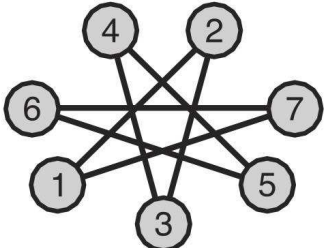
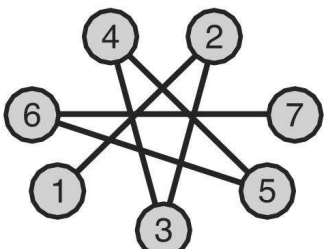
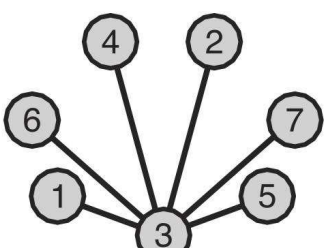
Topology	Group 1							Group 2								
<p>Complete graph</p> 		1	2	3	4	5	6	7		1	2	3	4	5	6	7
	1	-	91₅	94₄	94₄	90₇	86₁₃	93₄	1	-	89₁₀	92₁₁	94₃	92₁₁	92₁₁	91₉
	2	91₅	-	91₆	91₇	87₈	82₁₂	91₃	2	89₁₀	-	92₅	86₁₄	90₆	89₁₄	92₄
	3	94₄	91₆	-	95₂	94₂	85₁₃	94₃	3	92₁₁	92₅	-	92₁₁	93₄	91₁₃	92₆
	4	94₄	91₇	95₂	-	94₃	88₉	94₂	4	94₃	86₁₄	92₁₁	-	91₁₀	92₁₁	88₁₂
	5	90₇	87₈	94₂	94₃	-	84₁₂	91₄	5	92₁₁	90₆	93₄	91₁₀	-	92₁₃	92₅
	6	86₁₃	82₁₂	85₁₃	88₉	84₁₂	-	85₁₀	6	92₁₁	89₁₄	91₁₃	92₁₁	92₁₃	-	89₁₅
	7	93₄	91₃	94₃	94₂	91₄	85₁₀	-	7	91₉	92₄	92₆	88₁₂	92₅	89₁₅	-
<p>Ring graph</p> 		1	2	3	4	5	6	7		1	2	3	4	5	6	7
	1	-	74₂₈	59₃₁	59₂₇	47₂₆	65₂₈	75₂₄	1	-	77₂₃	63₂₈	61₂₉	65₂₉	78₁₆	86₁₂
	2	74₂₈	-	72₂₈	64₂₉	51₂₈	51₂₉	56₂₆	2	77₂₃	-	79₂₆	75₂₇	73₂₈	68₂₄	73₂₀
	3	59₃₁	72₂₈	-	84₁₈	67₂₇	60₃₅	59₂₉	3	63₂₈	79₂₆	-	91₁₄	81₂₁	61₂₇	64₂₂
	4	59₂₇	64₂₉	84₁₈	-	83₂₀	69₂₉	65₂₃	4	61₂₉	75₂₇	91₁₄	-	83₂₀	60₂₉	61₂₇
	5	47₂₆	51₂₈	67₂₇	83₂₀	-	78₂₅	63₂₃	5	65₂₉	73₂₈	81₂₁	83₂₀	-	69₃₁	68₂₆
	6	65₂₈	51₂₉	60₃₅	69₂₉	78₂₅	-	81₂₁	6	78₁₆	68₂₄	61₂₇	60₂₉	69₃₁	-	91₄
	7	75₂₄	56₂₆	59₂₉	65₂₃	63₂₃	81₂₁	-	7	86₁₂	73₂₀	64₂₂	61₂₇	68₂₆	91₄	-
<p>Path graph</p> 		1	2	3	4	5	6	7		1	2	3	4	5	6	7
	1	-	93₃	82₇	69₁₇	60₂₇	57₂₈	55₂₈	1	-	96₃	89₆	73₂₂	56₃₀	41₁₉	36₁₇
	2	93₃	-	89₅	75₁₆	65₂₄	62₂₆	60₂₇	2	96₃	-	93₅	73₂₆	58₃₂	43₂₀	37₁₈
	3	82₇	89₅	-	82₁₅	73₂₀	68₂₂	64₂₅	3	89₆	93₅	-	78₂₅	61₃₁	44₂₁	38₁₉
	4	69₁₇	75₁₆	82₁₅	-	89₁₂	84₁₃	79₁₆	4	73₂₂	73₂₆	78₂₅	-	74₂₁	49₁₉	41₁₈
	5	60₂₇	65₂₄	73₂₀	89₁₂	-	92₃	86₈	5	56₃₀	58₃₂	61₃₁	74₂₁	-	66₁₄	59₁₄
	6	57₂₈	62₂₆	68₂₂	84₁₃	92₃	-	94₃	6	41₁₉	43₂₀	44₂₁	49₁₉	66₁₄	-	88₈
	7	55₂₈	60₂₇	64₂₅	79₁₆	86₈	94₃	-	7	36₁₇	37₁₈	38₁₉	41₁₈	59₁₄	88₈	-
<p>Star graph</p> 		1	2	3	4	5	6	7		1	2	3	4	5	6	7
	1	-	91₅	93₄	92₅	91₃	86₁₃	72₂₅	1	-	94₄	97₁	96₁	97₁	94₂	94₂
	2	91₅	-	92₂	91₂	89₃	82₁₆	73₂₄	2	94₄	-	95₄	94₅	94₅	90₆	92₅
	3	93₄	92₂	-	96₁	95₂	87₁₆	76₂₄	3	97₁	95₄	-	97₁	98₁	94₂	95₂
	4	92₅	91₂	96₁	-	94₂	83₁₆	74₂₃	4	96₁	94₅	97₁	-	97₁	93₄	94₂
	5	91₃	89₃	95₂	94₂	-	84₁₅	73₂₅	5	97₁	94₅	98₁	97₁	-	94₂	94₂
	6	86₁₃	82₁₆	87₁₆	83₁₆	84₁₅	-	69₂₄	6	94₂	90₆	94₂	93₄	94₂	-	91₃
	7	72₂₅	73₂₄	76₂₄	74₂₃	73₂₅	69₂₄	-	7	94₂	92₅	95₂	94₂	94₂	91₃	-

Figure 10: Mean values and standard deviations, over the total number of eyes-open trials, of the *dyadic synchronisation index* obtained experimentally. Each row corresponds to one of the four implemented interaction patterns: topology representation (left column), indices for Group 1 (central column) and Group 2 (right column). Mean values and standard deviations (as subscripts) of $\rho_{d_{h,k}}$ are represented as percentiles for all the pairs of each topology and for both the groups, with bold values referring to pairs who were visually coupled in the experiments (i.e., there exists a link between the two agents in the respective topology representation).